Multi-decadal Records of Stratospheric Composition and their Relationship to Stratospheric Circulation Change

Anne R. Douglass[1], Susan E. Strahan[1,2], Luke D. Oman[1], Richard S. Stolarski[3]

[1]Atmospheric Chemistry and Dynamics Laboratory, NASA Goddard Space Flight Center, Greenbelt, MD, USA
[2]Universities Space Research Association, Columbia, MD, USA
[3]Department of Earth and Planetary Sciences, Johns Hopkins University, Baltimore, MD, USA

Correspondence to: Anne R. Douglass (Anne.R.Douglass@nasa.gov)

Abstract. Constituent evolution for 1990 – 2015 simulated using the Global Modeling Initiative Chemistry and Transport Model driven by meteorological fields from the Modern-Era Retrospective analysis for Research and Applications Version 2 (MERRA-2) is compared with three sources of observations: ground based column measurements of HNO_3 and HCl from two stations in the Network for the Detection of Atmospheric Composition Change (NDACCC, ~1990 – ongoing); profiles of CH_4 from the HALogen Occultation Experiment (HALOE) on the Upper Atmosphere Research Satellite (UARS, 1992 – 2005); profiles of N_2O from the Microwave Limb Sounder on the Earth Observing System satellite Aura (2005 – ongoing). The differences between observed and simulated values are shown to be time dependent, with better agreement after ~2000 compared with the prior decade. Furthermore, the differences between observed and simulated HNO_3 and HCl columns are shown to be correlated with each other, suggesting that issues with the simulated transport and mixing cause the differences during the 1990s and that these issues are less important during the later years. Because the simulated fields are related to mean age in the lower stratosphere, we use these comparisons to evaluate the time dependence of mean age. The ongoing NDACC column observations provide critical information necessary to substantiate trends in mean age obtained using fields from MERRA-2 or any other reanalysis products.

1 Introduction

The composition of the stratosphere is changing in response to changes in ozone depleting substances (ODSs), nitrous oxide (N_2O) and methane (CH_4) with consequences for the ozone layer, stratospheric circulation, stratosphere-troposphere exchange, and climate. Ozone depleting substances (primarily chlorine and bromine containing compounds) are decreasing due to cessation of their production as a result of the Montreal Protocol and its amendments. These man-made compounds are also greenhouse gases [Ramanathan, 1975] along with N_2O and CH_4 that are the sources of nitrogen and hydrogen radicals. The concentrations of N_2O and CH_4 are presently increasing as discussed for recent decades by Carpenter and Reimann [2014] and reflected in boundary conditions that are prescribed for the simulations (section 3). The stratospheric climate is changing in response to composition change, as increased greenhouse gases both cool the stratosphere and accelerate the stratospheric circulation [Butchart and

Scaife, 2001]. Both decreases in ODSs and cooling due to the increase in greenhouse gases cause ozone to increase by reducing ozone loss. Acceleration of the circulation causes column ozone to decrease in the tropics and increase at middle and high latitudes [Li et al., 2009]. The net ozone layer response is a combination of photochemical and dynamical changes, as well as feedbacks in ozone heating and photochemistry that link them.

Future evolution of the ozone layer is commonly investigated using three-dimensional chemistry climate models (CCMs) that combine a general circulation model (GCM) with a representation of photochemical and radiative processes. A common feature of middle atmosphere GCMs (without interactive chemistry) and CCMs (with interactive chemistry) is the intensification of the Brewer Dobson circulation (BDC) in the 21st century due to increases in greenhouse gases [Butchart et al., 2006]. BDC strengthening could manifest itself in many ways that impact ozone. Some observations in the tropics support BDC acceleration during the past few decades, but overall attempts to verify this prediction of models with measurements has resulted in mixed conclusions, as exemplified in the following paragraphs.

Kawatani and Hamilton [2013] find that tropical radiosonde observations for 1953 – 2012 show weakening of the quasi-biennial oscillation (QBO) that is consistent with increased tropical upwelling. Thompson and Solomon [2009] argue that for 1979-2006 Microwave Sounding Unit channel 4 temperature retrievals and the merged total ozone data set [McPeters et al., 2013; Frith et al., 2014] are consistent with BDC acceleration after accounting for the effects of volcanic eruptions. Integrated ozone profiles from the Stratospheric Aerosol and Gas Experiment (SAGE I and SAGE II) show ozone decreases of about 10 Dobson Units (DU) between 1979 and 2005 [Randel and Wu, 2007], consistent with decreases in tropical lower stratospheric ozone from a record for 1984-2009 obtained by combining SAGE II data with SHADOZ ozonesondes [Randel and Thompson, 2011], but inconsistent with the nearly constant timeseries of tropical total column ozone [Pawson and Steinbrecht, 2015]. Tropical lower stratospheric ozone increases measured by the SCanning Imaging Absorption SpectroMeter for Atmospheric CHartographY (SCIAMACHY), an instrument on Envisat (2002-2012), are also not consistent with a predicted circulation increase [Gephardt et al., 2014]. Harris et al. [2015] report no statistically significant O_3 trend in the tropical lower stratosphere. Simulations reported by Shepherd et al. [2014] produce an increase in tropospheric ozone that compensates for the stratospheric decrease, potentially resolving the discrepancy between the total column ozone record and the records that combine SAGE II with SAGE I or SHADOZ. Polvani et al. [2017] find that the ODSs themselves are primary drivers of tropical upwelling, in which case the decrease in ODSs over the coming decades will counter or reverse the impact of other greenhouse gases on the circulation. The future evolution of tropical column ozone is complex, and may be influenced by circulation change, by changes in tropospheric pollution, or both.

In the extratropics, intensification of the BDC will alter the distributions of source gases, including anthropogenic chlorofluorocarbons [Butchart and Scaife, 2001], increase the mid-latitude stratosphere-to-troposphere ozone flux [Hegglin and Shepherd, 2009] and decrease the stratospheric mean age [S. Li and Waugh, 1999; Austin and F. Li, 2006]. Although all CCMs predict increased tropical upwelling in the 21st century, both the rate of tropical increase

and the response of the extratropical circulation differ substantially. Douglass et al. [2014] show that differences in the details of the intensification of the extratropical circulation make major contributions to the spread in the stratospheric ozone level projected for 2100 obtained from the CCMs that contributed to a comprehensive effort to evaluate these models [SPARC CCMVal, 2010] and the Scientific Assessment of Ozone Depletion: 2010 [WMO, 2011].

There have been efforts to quantify BDC trends and variability as expressed in meteorological analyses. Diallo et al. [2012] report statistically significant negative age trends in the extratropics using meteorological fields from ERA-Interim for 1989-2010. Abalos et al. [2015] find common features that support negative age trends in the advective Brewer Dobson circulation for 1979 – 2012 in ERA-interim, the Modern-Era Retrospective analysis for Research and Applications (MERRA) and Japanese 55-year Reanalysis for 1979-2012. Ploeger et al. [2015] use the Chemical Lagrangian Model of the Stratosphere (CLaMS), driven by ERA-Interim reanalysis, to show how changes in both mixing and the residual circulation contribute to trends in age of air. Any of these results would be affected by changes in the observing system, and Diallo et al. [2012] caution that such changes may lead to false trends in the age obtained from analyzed fields. They emphasize the need for comparisons with trends derived from tracer observations. Furthermore, deficiencies in the GCM component of a reanalysis system such as lack of a spontaneous QBO may lead to spurious tropical ascent and subtropical mixing, also contributing to false trends [Tan et al., 2004; Coy et al., 2016].

Long-lived constituents (e.g., $CFCl_3$, CF_2Cl_2, N_2O), reservoir species that are products of their destruction (e.g., HNO_3 and HCl), and age tracers like SF_6 and CO_2 all carry information about changes in the circulation and mixing [Hall, 2000]. Engel et al. [2009] find no statistically significant trend in the northern midlatitude mean age derived from sparse balloon profiles of SF_6 and CO_2 between 1985 and 2005. Ray et al. [2010] used the same observations and trends in the tropical vertical velocity obtained from reanalysis datasets to show how trends in both horizontal mixing and upwelling affect the mid-latitude age trends, and find that the age changes indicated by the measurements differ from those produced by the CCMVal models. Garcia et al. [2011] show the importance of accounting for non-linear growth rates of the age tracers when comparing simulated ages with those derived from balloon observations. Ray et al. [2014] identify seasonal, quasi-biennial and decadal scales of variability in the middle latitude mean age by extending their previous analysis, accounting for variable growth rates in SF_6 and CO_2 and adjusting the measurement-based mean ages to a common equivalent latitude that is representative of the northern hemisphere.

Prior use of source gases to infer variability in mean age is limited. Schoeberl et al. [2005] explored the relationship between mean age and trace gas distributions in a chemistry and transport model (CTM) driven by winds from a general circulation model, interpreting their results using observations of CH_4, N_2O, and chlorofluorocarbons CF_2Cl_2 and $CFCl_3$ from the Cryogenic Limb Array Etalon Spectrometer (CLAES) on NASA's Upper Atmosphere Research Satellite [Roche et al., 1996] and from the Atmospheric Chemistry Experiment-Fourier Transform Spectrometer (ACE-FTS) on the Canadian SciSat [Bernath et al., 2005]. They associate young mean ages with high values of tracers seen by CLAES at the northern lower middle latitudes in 1993, and older mean ages with lower values for ACE-FTS

tracers in 2005, speculating that the different relationships during these two periods are evidence of quasi-biennial variability in the mean age. Strahan et al. [2015] showed the signature of the QBO in the variability of the southern midlatitude middle stratosphere N_2O and mean age using 9 years of observations from the Microwave Limb Sounder (MLS) on NASA's Earth Observing System (EOS) Aura.

A recent analysis of HCl column measurements from stations in the Network for the Detection of Atmospheric Composition Change (NDACC) highlights the relationship between mean age, low frequency variability and the HCl column amounts. Both satellite and ground-based observations show an increase in northern hemisphere (NH) column and lower stratospheric HCl between 2007 and 2011 [Mahieu et al., 2014]. CTM simulations using meteorological fields from ERA-Interim reproduce the lower stratospheric pattern of NH HCl increase and southern hemisphere (SH) decrease, consistent with an increase in the mean age and a slowdown in the NH mid-latitude lower stratospheric circulation. The HCl increase indicates air with older mean age that has spent more time at higher altitudes [Hall, 2000] where it experiences rapid chlorofluorocarbon destruction leading to higher levels of HCl. The magnitude and duration of the HCl column increase attests to the importance of quantifying the natural variability that produced it. Large natural multi-annual variations make it more difficult to quantify trends in the circulation, to identify a decrease in inorganic chlorine caused by the decrease in ODSs, or to attribute an ozone increase to ODS decrease.

The goal of this work is to use multi-decadal observations of source and reservoir trace gases from satellite and ground-based instruments, along with a hindcast simulation from the Global Modeling Initiative chemistry and transport model (GMI CTM), driven by meteorological fields from MERRA Version 2 (MERRA-2), to explore extratropical variability and trends in lower stratospheric transport and mean age between 1990 and 2015. This work establishes a framework for the use of ground-based and satellite observations of constituents other than ozone to identify and quantify long-term changes in the residual circulation. We argue that the simulation must reproduce the interannual and longer time scale variability seen in the observed data records to confirm the realism of trends in the simulated mean age. We consider two overarching questions:

1) Do comparisons of modeled and observed trace gases support the trends in circulation and mean age inferred from reanalyses?

2) Are the on-going sparse datasets available from the early 1990s sufficient to characterize multi-year variability and thereby provide more robust trend estimates?

Observations used in this work include columns of reservoir gases at several NDACC stations (~1990 – ongoing), profiles from the HALogen Occultation Experiment (HALOE) on the Upper Atmosphere Research Satellite (UARS) (1991 – 2005), and near global profile datasets from the Microwave Limb Sounder (MLS) on Earth Observing System (EOS) Aura (mid 2004 – ongoing); these are described in section 2. Models are discussed in section 3. Comparisons of simulations with observations and their relationship to simulated mean age are found in section 4. Discussion and conclusions follow in section 5.

2 Observations

2.1 Network for the Detection of Atmospheric Composition Change

Here we use total column measurements of HCl described by Mahieu et al. [2014] and version 7 HNO_3 [Ronsmans et al., 2016] from Fourier Transform InfraRed (FTIR) instruments at two stations (Jungfraujoch, Switzerland, 46.6° N 7.98° E and Lauder, New Zealand, 45.0° S 169.7° E). Both of these stations belong to the Network for the Detection of Atmospheric Composition Change (NDACC; http://www.ndacc.org). The data, courtesy of Emmanual Mahieu (PI for the NDACC Jungfraujoch station) and Dan Smale (PI for the NDACC Lauder station), are publicly available through anonymous ftp at ftp://ftp.cpc.ncep.noaa.gov/ndacc/station/jungfrau/ and ftp://ftp.cpc.ncep.noaa.gov/ndacc/station/lauder/. This analysis is limited to mid-latitudes, and these stations are chosen for comparison with the simulation because of the length of their records (~1987 – ongoing at Jungfraujoch, and ~1990 – ongoing at Lauder). The comparison of the simulation with data from other northern mid-latitude stations is similar to that reported here, but not discussed here because the length of record is important to this analysis.

2.2 UARS HALogen Occultation Experiment (HALOE)

The Halogen Occultation Experiment (HALOE) on the Upper Atmosphere Research Satellite (UARS) [Russell et al., 1993] measured profiles of ozone and other gases including methane (CH_4) using solar occultation from September 1991 until end-of-mission in late 2005. HALOE nominally obtained 15 sunrise and sunset profiles daily, providing near global coverage in about a month. HALOE obtained profiles between 270 and 320 days/year between 1992 and 1995, but operational issues limited measurements to about 180 days/year for 1996 until end of mission in November 2005. These issues precluded observations during some seasons at specific latitude bands later in the mission. We take this into account by restricting comparisons with the simulation to winter between 35° and 55° latitude where the number of observations/year is nearly constant in both hemispheres. Profiles used here are retrieved using algorithm version 19 and interpolated to 13 UARS standard pressure levels starting at 100 hPa (i.e., p_i=100*exp(i/6) where i is an integer). The combined systematic and random uncertainty of single CH_4 profiles in the lower stratosphere is 11–19% [Grooß and Russell, 2005].

2.3 Aura Microwave Limb Sounder (MLS)

Livesey et al. [2017] describe the version 4.2 (V4) Microwave Limb Sounder (MLS) data products, their precision, accuracy, and screening procedures to identify and eliminate profiles that are not recommended for scientific use. Here we use MLS observations for 2005 – 2015 for the source gas nitrous oxide (N_2O). The V4 dataset retrieved from the band 12 640-GHz (N_2O-640) is scientifically useful from 100 hPa to 0.46 hPa. This dataset begins shortly after launch but ends in mid-2013 due to band failure. The second V4 dataset, retrieved from band 3 190-GHz (N_2O-190), begins shortly after launch and is ongoing. Aura MLS provides ~3495 profiles daily between 81°S and 81°N; data are averaged in 2° latitude bins (30-60 profiles per bin after screening), reducing precision uncertainty. Monthly,

seasonal and annual averages are compared with simulations that are described below. The highest pressure level for useful measurements is 68 hPa for N_2O-190 compared with 100 hPa for N_2O-640. In addition, percentage differences (N_2O-190 - N_2O-640)/N_2O-640*100 vary both seasonally and temporally at middle latitudes. For example, NH monthly zonal mean differences at 68 hPa are between 4 and 8 percent in 2005 and decrease to 0 – 5% by 2012, with greater temporal dependence during winter months. We limit comparisons with simulated N_2O to 46.4 hPa and lower pressures where the bias and its temporal dependence are smaller.

3 Models

3.1 GMI CTM

A GMI CTM hindcast simulation was integrated January 1 1980 – 2015 using MERRA-2 meteorological fields [Gelaro et al., 2017]. MERRA-2 ingests recent satellite observations and uses an improved general circulation model [Molod et al., 2015] compared with the MERRA [Rienecker et al., 2011]. This GMI CTM simulation has 2^o lat x 2.5^o lon horizontal resolution and 72 vertical levels having ~1 km resolution between 300 and 10 hPa. Details of a similar GMI CTM simulation using the earlier MERRA fields at 1^o lat x 1.25^o lon resolution are found in Strahan et al. [2013] and references therein. Reaction rates and cross sections are from the JPL evaluation 18 [Burkholder et al., 2015]. Surface mixing ratio boundary conditions for all organic halogen and long-lived source gases follow the WMO A1 2010 and RCP8.5 scenario, respectively, and include 5 ppt additional CH_3Br to account for bromine from short-lived source gases. Time-dependent stratospheric aerosols come from IGAC as prescribed for the SPARC Chemistry Climate Model Initiative (CCMI) simulations. The simulation was initialized with December 1979 MERRA-2 meteorological fields using source gas and reservoir constituent fields from a prior simulation. The same MERRA-2 meteorological fields were used to integrate a clock tracer. The clock tracer is a linearly increasing conservative transport tracer forced at the two lowest model levels and has no atmospheric losses. It is always reset to the current date at the surface.

3.2 GEOSCCM

The Goddard Earth Observing System Chemistry Climate Model (GEOSCCM) couples the GEOS version 5 general circulation model [Rienecker et al., 2008; Molod et al., 2012] to the (GMI) stratosphere-troposphere chemical mechanism [Duncan et al., 2007; Strahan et al., 2007; Oman et al., 2013]. The simulation used is run on the cubed sphere at c48 resolution, equivalent to a 2° horizontal resolution, with the same vertical layers as GMI CTM. The surface mixing ratio boundary conditions are the same, except GEOSCCM uses the WMO A1 2014 halogen scenario instead of the A1 2010 used in the GMI CTM (these are very similar). Reaction rates and cross sections are the same as described for the GMI CTM. Observed sea surface temperatures and sea ice concentrations are also used to force this free-running simulation [Rayner et al., 2003].

4.0 Results

The global daily observations of the long-lived tracer N_2O obtained from MLS are ideal to determine whether circulation trends inferred from analyses and/or from simulated age of air trends are consistent with observations. The MLS dataset began in mid-2004 and is ongoing, but the projected changes in the BDC are multi-decadal. We therefore consider whether the sparse datasets available from the early 1990s are sufficient to characterize multi-annual variations, piecing together space-based observations from UARS HALOE and the multi-decadal ground-based column measurements of HNO_3 and HCl. For 2005 onward we test whether information from the ground-based column measurements is consistent with that obtained from MLS.

The first step towards meeting these goals is to examine the relationships between tracer and reservoir species and the mean age as produced by simulations using the GMI CTM and the GEOSCCM (section 4.1). Our focus in section 4.2 is to test whether the simulated changes track the observations of CH_4 (UARS HALOE), N_2O (Aura MLS), and of reservoir gases HCl and HNO_3 from 1987 – present (NDACC ground based column measurements).

4.1 Relationships among simulated age, N_2O, CH_4 and reservoir gases

4.1.1 Source gases N_2O and CH_4

Strahan et al. [2011] show that N_2O observations from ACE-FTS are anti-correlated with mean age observations for N_2O values less than 150 ppbv and mean age less than 4.5 years. Here we focus on the relationship between annual mean values to emphasize interannual and longer time scale variability in circulation, noting that peak-to-peak seasonal variations in N_2O and CH_4 (~10% of their respective means) and age (~20% of mean) are also anti-correlated (not shown). Examples of the evolution of annual mean age, N_2O and CH_4 in the GMI CTM, driven by MERRA-2 winds, show that mean age is anti-correlated with both N_2O and CH_4 (Fig. 1(a) and Fig. 1(b)).

The GMI CTM results show a large N_2O increase between ~1987 and ~1995 in the northern mid-latitudes followed by a decrease from 2002-04 through 2010, and another increase from 2010 to 2013. These are indicators of multi-year variability in MERRA-2 transport. The evolution of CH_4 parallels that of N_2O after about 1987. The relationship between these tracers and age is similar in the SH, with shorter periods of smaller increases or decreases in both tracers compared with the NH. Annual mean N_2O changes are generally reflected in the time series of annual mean age; the correlation coefficients between N_2O and mean age for this example are -0.77 (NH) and -0.66 (SH).

Comparison of the evolution of mean age, N_2O and CH_4 in the GMI CTM (Fig. 1(a) and Fig. 1(b)) with that in the GEOSCCM (Fig. 1(c) and Fig. 1(d)) illuminates dynamical differences between the models as the simulations use the same boundary conditions for these gases. GEOSCCM changes in N_2O and CH_4 are reflected in the time series of

mean age (correlation coefficients between annually averaged N_2O and age are -0.91 in the NH and -0.96 in the SH), but the multi-year variability is smaller. The percentage change per decade is calculated for successive 10-year periods beginning in 1980 for both hemispheres (Fig. 1(e) and Fig. 1(f)). In GEOSCCM, the rate of N_2O increase in the extratropics is always close to the tropical rate of increase of ~2.6%/decade, with a small signature of the effect of the Pinatubo aerosols on the circulation. In contrast, the decadal rate of change in the GMI CTM extratropics may be 2 – 3 times greater or of the opposite sign compared with the rate of increase at the tropical tropopause (the same in both simulations as it is controlled by the boundary condition).

4.1.2 Mean Age and Fractional Release

The age spectrum for a stratospheric air parcel is the distribution of transit times between entry to the stratosphere to the parcel location for each of the elements that comprise the parcel. The mean age is the average of this distribution, and comparisons of simulated mean age with that obtained from measurements such as SF_6 (a long-lived trace gas that is increasing in the troposphere) provide information about the realism of the advective and mixing processes that control the parcel paths. Hall et al. [1999] used mean age comparisons to show lack of realism in the transport produced by various models that participated in Model and Measurements Intercomparison II [Park et al., 1999]. Hall [2000] and Schoeberl et al. [2000] used trajectory calculations to show on average, the oldest elements have risen to highest altitudes, thus evidence of loss of a long-lived gas in a parcel found in the lower stratosphere indicates that the age spectrum includes parcel elements that have experienced high altitude where source gas destruction occurs. These older elements of the age spectrum contribute to the mean age and determine the amount of destruction of long-lived gases. This relationship between the oldest elements of the age spectrum and the probability of destruction leads to compact, inverse relationships between mean age and gases with tropospheric sources. Indeed, aircraft observations show that the destruction of long-lived gases including chlorofluorocarbons, N_2O and CH_4 is related to the mean age obtained from SF_6. Schauffler et al. [2003] use aircraft observations to compute the fractional release f_r

$$f_r = \left(1 - \frac{X(\mathbf{x})}{X_i}\right)$$

where $X(\mathbf{x})$ is the mixing ratio of a source gas in a parcel at location $\mathbf{x}$ (latitude, altitude, pressure, time) and X_i is the mixing ratio at entry to the stratosphere, finding a near linear relationship between fr and the SF_6 mean age. Waugh and Hall [2002, and references therein] discuss the relationship between tracer distributions and transport timescales in the stratosphere, noting the connection between the BDC and the wave-driven quasi-horizontal mixing that control distributions of stratospheric trace gases. Because the fractional release depends on destruction of the source gas and therefore on the portion of the age spectrum that reaches high altitude where destruction is possible, the relationship between fractional release and mean age is a stronger test of the realism of simulated transport than the simple comparisons of mean age distributions. The older elements of the age spectrum that contribute to the mean age make

the largest contribution to the fractional release. Mean age is negatively correlated with source gases and positively correlated with the products of their destruction (e.g., HCl and HNO_3).

In GEOSCCM the BDC is fully consistent with the planetary wave breaking that results in horizontal mixing and plays a role in driving the BDC. This consistency is not guaranteed in the MERRA-2 fields. Comparison of fractional release and its relationship to mean age with values obtained from observations tests the balance between horizontal mixing and vertical transport. Waugh et al. [2007] apply these concepts to the simulated amounts of inorganic chlorine (Cl_y) released from source gases in a CTM using different grid resolution and meteorological fields, finding large differences in Cl_y for the same mean age. Within the same CTM, different meteorological fields or different implementation of meteorological fields may produce the same mean age but different values for the fractional release because the mean transport pathways differ.

In GMI CTM the fractional release of N_2O for fixed mean age varies substantially between 1990 and 2000 in both hemispheres (Fig. 2(a) and Fig. 2(b)). In contrast, in GEOSCCM the fractional release at fixed mean age varies slowly (Fig. 2(c) and Fig. 2(d)). The changing relationship between fractional release and mean age in the GMI simulation reveals decadal variations in the relationship between horizontal and vertical transport processes in MERRA-2. After about 2000, the small variations in fr for fixed mean age in GMI CTM are comparable to the variations obtained throughout the period for GEOSCCM. We illustrate this by comparing the ratio of the fr standard deviation to its mean for 1990 – 2000 and 2005 – 2015 for each simulation for both hemispheres (Fig. 2(e) and Fig. 2(f)). In GEOSCCM the ratio is about 2% for both time periods and for both hemispheres. For GMI CTM the ratio for 1990 – 2000 is between 6% and 8% for the age range 2 – 3.5 years in both hemispheres. For 2005 – 2015 the GMI CTM ratio is comparable to that obtained from GEOSCCM, although still larger than GEOSCCM in the southern hemisphere. The smaller values of fr at fixed mean age found during the early 1990s suggest that the balance between horizontal and vertical transport processes up until about 2000 is substantially different in both hemispheres in the first half of the 1990s than in subsequent years. This changing relationship contributes to the lower correlations of mean age with long-lived tracers in GMI CTM compared with GEOSCCM noted in section 4.1.1 and also affects the relationship of mean age with reservoir gases discussed below.

4.1.3 Reservoir gases HCl and HNO_3

Hydrochloric acid is the most abundant of the chlorine product species throughout the stratosphere, and more than 80% of the HCl column resides below 20 hPa. The sources of HCl increased by ~5%/year up until about 1992 but leveled off during the late 1990s. The long-lived gases $CFCl_3$ and CF_2Cl_2 have been decreasing slowly since ~2000 (<1%/year) due to cessation of ODS production as a result of the Montreal Protocol and its amendments. Methyl chloroform (CH_3CCl_3) is shorter lived, and contributed about ~15% of total inorganic chlorine in the lower stratosphere in 1995, decreasing rapidly thereafter. Prior to ~2000, growth of the HCl column and the HCl lower stratospheric mixing ratio was controlled by the rapid growth of the source gases.

After ~2000, the simulated evolution of lower stratospheric HCl and its column broadly match mean age in both hemispheres (Fig. 3), although neither is a perfect surrogate for mean age variability at a particular level. Multiyear changes in the mid-latitude HCl columns that are larger or opposite in sign to the source gas decrease reflect changes in the residual circulation [Mahieu et al., 2014]. This is seen in the southern hemisphere, where simulated column decreases are more rapid than can be accounted for by the decrease in source gases between 2005 and 2011. During this period the SH mean age decreases throughout the lower stratosphere (maximum rate of decrease 1%/year at 100 hPa), contributing to the decrease in simulated HCl column.

Nitric acid is similar to HCl in that both are produced from radicals released by destruction of tropospheric source gases in the upper stratosphere. It is the dominant component of total odd nitrogen (NO_y) between the tropopause and ~50 hPa, poleward of about 40° in both hemispheres. Lower stratospheric N_2O is anti-correlated with NO_y and also with HNO_3 during winter when HNO_3 is ~90% of NO_y. The stratosphere below 50 hPa contains ~80% of the total winter column HNO_3. Except when the lower stratospheric aerosol layer is enhanced by a Pinatubo-type volcanic eruption, a 'trend' in the residual circulation may be identified by an increase in middle latitude HNO_3 columns that is faster or slower than the trend in N_2O increase (~0.3%/yr) for several consecutive years. The HNO_3 column, lower stratospheric HNO_3 mixing ratio and the mean age simulated using GMI CTM track one another at middle latitudes in both hemispheres starting in 1993, about 18 months after the eruption of Mt. Pinatubo (Fig. 4).

Although neither the total column HNO_3 or HNO_3 mixing ratio at a particular level correlates perfectly with the mean age, Fig. 4 shows decadal scale upward trends in both hemispheres in HNO_3 column, HNO_3 mixing ratio and mean age for ~1998 to 2010. The simulated winter HNO_3 mixing ratio and mean ages are correlated with levels above and below, and with each other between 25-85 hPa. The column, mean age and lower stratospheric mixing ratio are positively correlated throughout the middle latitudes of both hemispheres.

4.2 Observations, GMI CTM simulation, and Mean Age

The relationships of constituents and mean age apparent in the GMI CTM simulation driven by MERRA-2 fields suggest that quantitative information about residual circulation change at middle latitudes can be obtained from existing and on-going measurements. The following discussion considers the northern and southern hemispheres separately. In each we compare the simulation with ground-based FTIR column measurements of reservoir gases HCl and HNO_3, available from the early 1990s at some stations, with HALOE measurements of the source gas CH_4 (1992 – 2005) and with Aura MLS measurements of N_2O (2005 – present).

4.2.1 Northern Hemisphere

NDACC – Jungfraujoch, Switzerland (46.6° N 7.98° E)

When sampled for the time and location of the observations, the northern hemisphere NDACC column observations of HNO_3 and HCl are highly correlated with the GMI columns (Fig. 5). These scatter plots include daily and seasonal variability as well as any trend in HCl and HNO_3 due to trends in their source gases during the 26 years of measurements (1989 – 2014). The mean of the GMI HCl columns is within 3% of the mean of observations. The mean of the GMI HNO_3 columns is 21% lower than the mean of the observations.

The timeseries of differences between observed and simulated HCl columns reveals a bias that changes over the course of the integration (Fig. 6(a)). The simulation is low biased before 2000 (positive differences) but has greatly reduced bias after ~2004. The timeseries of differences between observed and simulated HNO_3 columns is similar to that of the HCl columns. The changing bias is demonstrated by comparing histograms of the percentage difference between observations and simulation for 1989-2004 and 2005 – 2015 (Fig. 6(b) and Fig. 6(c)). The bin size for each gas is equal to 1/3 of the standard deviation of all measurements. In both cases the distribution of differences for 1989 - 2004 is shifted towards the right compared with the distribution for 2005 – 2015. There are fewer observation days per year prior to 1996 (average 37, standard deviation 24) than 1997 onward (average 95, standard deviation 27), but subsampling later years to match the observation frequency and seasonality of early years does not change this result. The shift towards better agreement is not sensitive to the exact time interval (i.e., similar results are obtained comparing the distribution for 1989 – 2000 with 2000 – 2015. We chose to compare emphasize 2005 – 2015 because Aura MLS obtained global datasets during this period.

Figure 7 shows that on days when both HCl and HNO_3 are measured, the differences between measured and simulated HNO_3 are strongly correlated with the differences between measured and simulated HCl. This correlation is found whether daily, monthly or annual averaged time scales are considered. On the annual time scale, the correlation is found whether averaging all measurements for each gas each year or when averaging only measurements on days both gases were reported. We conclude that the similar time dependencies of the differences (ΔHCl and ΔHNO_3) are caused by substantial differences in the transport characteristics of MERRA-2 fields during the 1990s compared with the period 2004 and onward. The correlation between differences cannot be explained by photochemistry, because unrelated processes control partitioning of the chlorine and nitrogen containing reservoir species in the lower stratosphere. Furthermore, this correlation holds even though anthropogenic chlorine source gases increased until ~2000 and declined thereafter while the source gas N_2O increased steadily for the entire period. Our conclusion is consistent with the change in the relationship between the fractional release and mean age found in the northern hemisphere lower stratosphere (Fig. 2(a) and Fig. 2(e)). The lower values of fractional release during the 1990s are consistent with the shift in the distribution of HCl column differences from a low bias in the 1990s to a much smaller low bias after 2004. This also explains the shift in the distributions of HNO_3, but does not explain the low bias in simulated HNO_3 that remains after 2004 (20%) when the difference between simulated and observed HCl is within experimental error.

Aura MLS Northern Hemisphere

As discussed in detail by Strahan et al. [2011], the mean age is a near linear function of N_2O for N_2O values greater than about ~150 ppbv (about half the value at the tropical tropopause). Here we focus on midlatitude annual averages at two MLS levels (46.4 hPa and 31.8 hPa), noting that the difference between the simulated and zonal mean MLS N_2O (640 GHz receiver) is less than 10% for MLS annual means greater than 150 ppbv. To emphasize multi-year variations, we compare simulated annual averages with observed values from both MLS N_2O bands at 46° N at 46.4 hPa and 32 hPa (Fig. 8). There is a 6% bias between the annual means for N_2O-190 compared with N_2O-640 at 46.4 hPa. Simulated N_2O agrees well with observations throughout the period, and is strongly anti-correlated with the simulated mean age. The observed and simulated 2006 - 2011 decreases are accompanied by simulated increases in mean age, consistent with column increases in both HCl and HNO_3 [Mahieu et al., 2014].

UARS HALOE Northern Hemisphere

Because HALOE sampling is not uniform, the simulation output is sub-sampled at the location and time of the HALOE measurements. We focus on January-February-March for 35°-55° N because the number of profiles obtained at midlatitudes during each winter is similar over the life of the mission (see section 2.2).

Factors other than non-uniform sampling complicate the relationship of HALOE CH_4 with circulation and mean age. First, because aerosols from the eruption of Mt. Pinatubo interfere with HALOE measurements below 46 hPa in 1992 and 1993, we focus on comparisons at 46.4 hPa, 31.6 hPa and 21.5 hPa. Second, the rate of CH_4 increase at the tropical tropopause (specified by the boundary condition) is variable and may be substantially larger, about the same, or smaller than the rate of increase of N_2O (Fig. 1). The rate of CH_4 increase in the tropics at 100 hPa is greater than 1%/year in 1979, falls to less than 0.1%/year between 2000 and 2005, and increases to 1%/year by the end of the integration. Assuming that the observationally derived boundary condition is correct, comparisons of observed and simulated CH_4 test the fidelity of the transport. Finally, we note that normalized vertical and horizontal CH_4 gradients are smaller than the N_2O gradients, making CH_4 less sensitive to circulation changes.

The differences between HALOE and simulated CH_4 for 1992-1998 are compared with differences for 1999-2005 by examining histograms of the percentage differences for each time period at 46.4 hPa, 31.6 hPa and 21.5 hPa (Fig. 9). At all three levels, the distributions shift towards smaller difference in the later time period. The observed and simulated values are positively correlated for 1992-1998 (between 0.7 and 0.8), but correlations are larger during the later period (slightly larger than 0.8). The larger differences during the earlier period are consistent with greater horizontal mixing and with the unexpected time dependence in the relationship of fractional release and simulated mean age.

We look at observed and simulated CH_4 changes over the period of the HALOE observations by computing the difference between 1994-1999 and 2000-2005 mean profiles (Fig. 10). The HALOE mean CH_4 decreases between 68 hPa and 10 hPa, whereas the GMI CH_4 increases (Fig. 10(a)). The very small differences between HALOE and GMI at the two lowest levels suggest that the time dependence of the mixing ratio at stratospheric entry is realistic. The

simulated mean ages for 2000 – 2005 are younger for 68 hPa – 10 hPa compared with 1994-1999, consistent with the increase in GMI CH_4, however the HALOE data do not support this decrease in mean age as produced by the MERRA-2 meteorological fields.

To summarize the northern hemisphere comparisons, the simulated columns of HNO_3 and HCl follow NDACC observations at the Jungfraujoch station after ~2000 with higher fidelity than prior years. The simulated columns of both constituents are lower than the observed columns during the middle 1990s; this is consistent with lower values for fractional release for a given mean age in the 1990s compared with the 2000s (Fig. 2). The comparison of simulated CH_4 with HALOE observations similarly shows that the age change produced by the GMI CTM using MERRA-2 meteorology between 68 hPa and ~20 hPa during the 1990s is not realistic. The mean fractional release for fixed mean ages is larger after 2000 (Fig. 2(a)), indicating that after 2000 MERRA-2 transport pathways take more air parcels to higher altitudes than during the 1990s [Hall, 2000]. The simulated long-lived species HCl, HNO_3, CH_4 and N_2O are all closer to the observations after 2000, indicating transport characteristics of the GMI CTM using MERRA-2 are more realistic in this period.

Together, the observations do not support the MERRA-2 mean age evolution before 2000, but do support the realism of the increase in northern midlatitude lower stratospheric mean age between 2005 - 2011 following the quiescent period 2000 - 2004. The strong relationship between variability in simulated lower stratospheric mean age, MLS N_2O, and the NDACC HNO_3 columns demonstrates the value of these observations for evaluating the residual circulation and mixing in meteorological analyses. Furthermore, the duration of periods of positive or negative changes in the circulation shows that multi-decadal records are required to identify a geophysically significant trend in the stratospheric circulation.

4.2.2 Southern Hemisphere

NDACC Lauder, New Zealand (45.0° S 169.7° E)

As for the NH Jungfraujoch station, the simulation is sampled for the time and location of the HCl and HNO_3 column observations at the Lauder station. The simulated columns for both species are correlated with observations (Fig. 11(a) and Fig. 11(b)), although there is more scatter in the relationship between observed and simulated HCl columns evidenced by the lower SH correlation (0.73) compared with the NH (0.90). The mean bias between observations and simulation is less than 4% for HCl and about 18% for HNO_3, comparable to the NH. The distributions of differences shift slightly towards better agreement for 2004 – 2014 compared with 1990-2004. The shifts are smaller than found for the NH.

Like the NH, the differences between observed and simulated HNO_3 columns are correlated with the differences between observed and simulated HCl columns (Fig. 12) for daily values ($r = 0.62$), monthly averages ($r = 0.61$), or annual averages ($r = 0.71$).

Aura MLS Southern Hemisphere

As expected, at middle latitudes the annual means of GMI N_2O and mean age (shown at 46° S) are correlated at 46.4 hPa and 31.6 hPa (Fig. 13). The GMI N_2O tracks the observed N_2O-640 at both levels and N_2O-190 only at 31.6 hPa. At 31 hPa the two retrievals maintain a near constant bias as a function of time, whereas bias is year dependent at 46.4 hPa. At 46.4 hPa the simulated N_2O reflects some of the observed year-to-year differences and agrees better with N_2O-640, while at 31.6 hPa it agrees very closely with N_2O-190. At 31.6 hPa, both retrievals are consistent with the mean age changes between 2004 and 2015.

UARS HALOE Southern Hemisphere

We focus on SH winter months July-August-September for 35°-55° S because the number of profiles obtained at midlatitudes during each winter is similar over the life of the mission (see section 2.2). As in the NH, we compare the differences between HALOE and simulated CH_4 for 1992-1998 with 1999-2005 by examining histograms of the percentage differences for each time period at 46.4 hPa, 31.6 hPa and 21.5 hPa (Fig. 14). Again, the distributions shift towards smaller differences during the later time period. The observed and simulated values are positively correlated for 1992- 1998 (0.63 - 0.78 on the three levels); correlations are nearly unchanged in the later period. As in the NH, the comparison improves as the integration proceeds, consistent with the evolving relationship between mean age and fractional release discussed above.

As in Fig. 10, we look at mean age and observed and simulated CH_4 changes over the period of the HALOE observations (Fig. 15). The age increase below 50 hPa has little impact on the simulated profile change because the gradients are weak. The mean age for 2000 – 2005 is younger for 50 hPa – 10 hPa compared with 1994-1999. Both the observed and simulated profiles changes are positive, consistent with the age decrease, but the simulated change is substantially larger than that observed for most of the profile, casting doubt on the realism of the simulated age decrease (Fig. 10b).

To summarize, comparison of constituent evolution from four data sets (NDACC HNO_3 and HCl columns, HALOE CH_4, Aura MLS N_2O) with the GMI CTM simulation leads us to similar conclusions in both hemispheres regarding MERRA-2 transport. Horizontal transport and mixing during the 1990s generally lead to somewhat older mean age, but agreement with observations improves as the relationship between mean age and fractional release evolves in the 2000s. This indicates that transport in the GMI CTM using MERRA-2 becomes more realistic as the simulation progresses. Lower fractional release for a given mean age leads to underestimates of the reservoir species during the 1990s. Overall the differences between observed and simulated columns of HCl are correlated with the differences between observed and simulated HNO_3, strongly indicating transport as their cause, and casting doubt on MERRA-2 driven GMI CTM lower stratospheric mean ages in the 1990s. In contrast, the agreement with MLS N_2O during the Aura period, along with better agreement with observed HCl and HNO_3 columns, indicates the realism of age variations obtained from 2005 onward.

5 Discussion and Conclusions

Reanalysis datasets such as MERRA-2 depend on the data assimilation system, its general circulation model, and the datasets that are ingested by the system. Global datasets are of limited duration, and even though the same system is used to produce a multi-decadal reanalysis, differences in the quality and type of datasets that make up the observing system are unavoidable [Gelaro et al., 2017]. Such differences may lead to non-physical trends in analysis products and in constituents simulated using reanalysis meteorological fields in frameworks such as the GMI CTM. Although the relationship between the fractional release and mean age is expected to change in the midlatitude lower stratosphere if the BDC strengthens due to climate change [Douglass et al., 2008], the observations are not consistent with the large changes in fractional release for fixed mean age obtained during the 1990s using GMI CTM compared with the changes in GEOSCCM.

Global observations of tracers such as N_2O, obtained by Aura MLS since mid 2004, are ideal for evaluating the transport circulation in reanalysis datasets. The comparisons of simulated and observed fields demonstrated here for the annual averages midlatitudes in both hemispheres and in a previous work using MERRA during Arctic winter [e.g., Strahan et al., 2016] attest to the realism of MERRA and MERRA2 meteorological fields from 2004 - present. Apparent trends in constituents in both hemispheres, seen in MLS N_2O and ground based column measurements of HNO_3 and HCl, are consistent with the changes in the lower stratospheric residual circulation that caused an increase in mean age between 2007 and 2011 in the northern hemisphere accompanied by smaller and opposing transport and mean age changes in the SH [Mahieu et al., 2014].

For the 1990s, in contrast, comparison of the simulated values with HALOE CH_4 and ground based columns reveal multiple issues in both hemispheres. The MERRA-2 circulation produces multiyear constituent trends that are not observed. The comparisons are markedly better after 2000, strongly suggesting that differences in the observing system affect the MERRA-2 fields. The differences between observed and simulated HCl and HNO_3 are correlated with each other whether considering daily, monthly or yearly averages, strongly suggesting that issues with transport produced by GMI CTM using MERRA-2 fields cause the differences during the 1990s. The change in the simulated relationship between the fractional release and the mean age between the 1990s compared with later years suggests a difference in the mean parcel paths such that highest altitude reached by the older air in the 1990s is lower than in the 2000s. The underestimate of simulated HNO_3 and HCl in the 1990s seen in Fig. 6 is consistent with fewer elements in the age spectrum experiencing altitudes high enough for rapid destruction of source gases.

Understanding and accounting for these time-varying residual circulation trends is necessary for many applications: 1) to identify the expected decrease in stratospheric inorganic chlorine as the chlorine source gases decrease due to the Montreal Protocol and its amendments; 2) to identify and quantify the expected increase in stratospheric ozone due to the chlorine decrease, separate from multi-year variability in dynamics and transport; 3) to characterize and

quantify the change in the Brewer-Dobson circulation due to increasing greenhouse gases; and 4) to characterize and quantify the expected midlatitude increase in stratospheric ozone caused by the aforesaid change in Brewer-Dobson circulation. Because the comparisons of observed and simulated HCl and HNO_3 columns are consistent with comparisons of observed and simulated fields of source gases (HALOE CH_4, 1992 – 2005; MLS N_2O 2005 - ongoing), continuation of these columns data sets provides a robust means to evaluate the transport and mean age produced by reanalysis products in offline models such as the GMI CTM, including their effects on stratospheric ozone. Finally, periods of positive or negative constituent 'trends' due to transport variability may be 5 years or longer in both hemispheres; this observation supports the requirement for multi-decadal records in order to identify a geophysically significant trend in the stratospheric circulation.

Acknowledgements. We thank the NASA Atmospheric Composition Modeling and Analysis, Aura, and Modeling Analysis and Predictions programs for supporting this research. We also thank the NASA Center for Climate Simulation (NCCS) for providing high-performance computing resources. We thank Stephen Steenrod and Megan Damon for updates to and integration of the GMI chemistry transport model simulation used here. We thank Emmanuel Mahieu of the Institute of Astrophysics and Geophysics, University of Liège. for the Jungfrajoch FTIR data. The multi-decadal monitoring program of University of Liège at the Jungfraujoch station has been primarily supported by the Fonds (National) de la Recherche Scientifique (F.R.S.-FNRS) and Belgian Federal Science Policy Office (BELSPO) (both in Brussels, Belgium) and by the Global Atmosphere Watch programme of MeteoSwiss (GAW-CH). The International Foundation High Altitude Research Stations Jungfraujoch and Gornergrat (HFSJG, Bern) supported the facilities needed to perform the FTIR observations. We thank Dan Smale and the National Institute of Water and Atmospheric Research (NIWA) MIR-FTIR team for the Lauder FTIR data. The NIWA FTIR programme is funded through the New Zealand Government's core research grant framework from the Ministry of Business, Innovation and Employment.

References

Abalos, M., Legras, B., Ploeger, F. and W. Randel, W. J.: Evaluating the advective Brewer-Dobson circulation in three reanalyses for the period 1979–2012, J. Geophys. Res. Atmos., 120, 7534–7554. doi: 10.1002/2015JD023182, 2015.

Austin, J., and Li, F.: On the relationship between the strength of the Brewer-Dobson circulation and the age of stratospheric air, Geophys. Res. Lett., 33, L17807, doi:10.1029/2006GL026867, 2006.

Bernath P. F., C. T. McElroy,C. T., Abrams, M. C., Boone, C. D., Butler, M., Camy-Peyret, C., Carleer, M., C. Clerbaux, C., Coheur, P.-F., Colin, R.. DeCola, P., DeMazie`re, M., Drummond, J. R., Dufour, D., Evans, W. F. J., Fast, H., Fussen, D., Gilbert, K., Jennings, D. E., Llewellyn, E. J., Lowe, R. P., Mahieu, E., McConnell, J. C., McHugh, M.,. McLeod, S. D., Michaud R., Midwinter, C., Nassar, R., Nichitiu, F., Nowlan, C., Rinsland, C. P., Rochon, Y. J., Rowlands, N., Semeniuk, K., Simon, P., Skelton, R., Sloan, J. J., Soucy, M.-A., Strong, K., Tremblay, P., Turnbull, D., Walker, K. A., Walkty, I., Wardle, D. A., Wehrle, V., Zander, R. and Zou J.: Atmospheric Chemistry Experiment (ACE): Mission overview, Geophys. Res. Lett., 32, L15S01, doi:10.1029/2005GL022386, 2005.

Burkholder, J. B., Sander, S, P., Abbatt, J., Barker, J. R., Huie, R. E., Kolb, C. E., Kurylo, M. J., Orkin, V. L., Wilmouth, D. M., and Wine, P. H.: Chemical Kinetics and Photochemical Data for Use in Atmospheric Studies, Evaluation No. 18," JPL Publication 15-10, Jet Propulsion Laboratory, Pasadena, http://jpldataeval.jpl.nasa.gov, 2015.

Butchart, N. and Scaife, A. A.: Removal of chlorofluorocarbons by increased mass exchange between the stratosphere and troposphere in a changing climate, Nature 410, 799-802, doi:10.1038/35071047, 2001.

Butchart, N., Butchart N., Scaife, A. A., Bourqui, M., de Grandpre´, J., Hare, S. H. E., Kettleborough, J., Langematz, U., Manzini, E., Sassi, F., Shibata, K., Shindell, D., and Sigmond M.: Simulations of anthropogenic change in the strength of the Brewer-Dobson circulation, Clim. Dyn., 27, 727-741, doi:10.1007/s00382-006-0162-4, 2006.

Coy, L., Wargan, K., Molod, A., McCarty, W. R., and Pawson, S.: Structure and dynamics of the Quasi-Biennial Oscillation, J. Climate 29, 5339–5354, doi: 10.1175/JCLI-D-15-0809.1, 2016.

Diallo, M., Legras, B. and Chédin, A.: Age of stratospheric air in the ERA-Interim, Atmos. Chem. Phys., 12, 12133-12154, doi:10.5194/acp-12-12133-2012, 2012.

Douglass, A. R., Stolarski, R. S., Schoeberl, M. R., Jackman, C. H., Gupta, M. L., Newman, P. A., Nielsen, J. E., and Fleming, E. L.: Relationship of loss, mean age of air and the distribution of CFCs to stratospheric circulation and implications for atmospheric lifetimes, J. Geophys. Res., 113, doi:10.1029/2007JD009575, 2008.

Douglass, A.R., Strahan, S. E., Oman, L. D., and Stolarski, R. S.: Understanding differences in chemistry climate model projections of stratospheric ozone, J. Geophys. Res. Atmos., 119, 4922–4939, doi:10.1002/2013JD021159, 2014.

Duncan, B.N., Strahan, S. E., Yoshida, Y., Steenrod, S. D., and Livesey, N.: Model study of cross-tropopause transport of biomass burning pollution, Atmos. Chem. Phys., 7, 3713-3736, 2007.

Engel, A., Möbius, T., Bönisch, H., Schmidt, U., Heinz, R., Levin, I., Atlas, E., Aoki. S., Nakazawa, T., Sugawara, S., F. Moore, F., D. Hurst, D., J. Elkins, J., Schauffler, S., Andrews, A., and Boering, K.: Age of stratospheric air unchanged within uncertainties over the past 30 years, Nature Geosci., 2, 28-31, doi: 10.1038/NGEO388, 2009.

Frith, S. M., Kramarova, N. A., Stolarski, R. S., McPeters, R. D., Bhartia, P. K., and Labow, G. J.: Recent changes in total column ozone based on the SBUV Version 8.6 Merged Ozone Data Set, J. Geophys. Res. Atmos., 119, 9735-9751, doi:10.1002/2014JD021889, 2014.

Garcia, R. R., Randel, W. J. and Kinnison, D. E.: On the determination of age of air trends from atmospheric trace species, J. Atmos. Sci., 68, 139-154, doi: 0.1175/2010JAS3527.1, 2009.

Gebhardt, C., Rozanov, A., Hommel, R., Weber, M., Bovensmann, H., Burrows, J. P., Degenstein, D., Froidevaux, L. and Thompson, A. M.: Stratospheric ozone trends and variability as seen by SCIAMACHY from 2002 to 2012, Atmos. Chem. Phys., 14, 831-846, doi:10.5194/acp-14-831-2014, 2014.

Gelaro, R., et al.: The Modern-Era Retrospective Analysis for Research and Applications, Version 2 (MERRA-2). J. Climate, 30, 5419–5454, https://doi.org/10.1175/JCLI-D-16-0758.1, 2017.

Grooß, J.-U. and Russell III, J. M.: Technical note: A stratospheric climatology for O_3, H_2O, CH_4, NO_x, HCl and HF derived from HALOE measurements, Atmos. Chem. Phys., 5, 2797-2807, doi:10.5194/acp-5-2797-2005, 2005.

Hall, T. M.: Path histories and timescales in stratospheric transport: Analysis of an idealized model, J. Geophys. Res., 105(D18), 22811–22823, doi:10.1029/2000JD900329.

Harris, N. R. P. et al.: Past changes in the vertical distribution of ozone – Part 3: Analysis and interpretation of trends, Atmos. Chem. Phys., 15(17), 9965–9982, doi:10.5194/acp-15-9965-2015, 2015.

Hegglin, M. I. and Shepherd, T. G.: Large climate-induced changes in ultraviolet index and stratosphere-to-troposphere ozone flux, Nature Geo., 2, 687-691, 2009.

Kawatani, Y., and Hamilton, K.: Weakened stratospheric quasibiennial oscillation driven by increased tropical mean upwelling, Nature 497, 478-481, doi:10.1038/nature12140, 2013.

Li, S., and Waugh, D. W: Sensitivity of mean age and long-lived tracers to transport parameters in a two-dimensional model, J. Geophys. Res., 104(D23), 30559–30569, doi: 10.1029/1999JD900913, 1999.

Livesey, N., Read, W. G., Wagner, P. A., Froidevaux, L., Lambert, A., Manney, G. L., Milla´n Valle, L. F., Pumphrey, H. C., Santee, M. L., Schwartz, M. J., Wang, S., Fuller, R. A., Jarnot, R. F., Knosp, B. W., Martinez, E.: Earth Observing System (EOS) Aura Microwave Limb Sounder (MLS) version 4.2x level 2 data quality and description document JPL D-33509 Rev C, 2017.

Mahieu, E., Chipperfield, M. P., Nothold, J., Reddmann, T., Anderson, J., Bernath, P. F., Blumenstock, T., Coffey, M. T., Dhomse, S. S., Feng, W., Franco, B., Froidevaux, L., Griffith, D. W. T., Hannigan, J. W., Hase, F., Hossaini, R., Jones, N. B., Morino, I., Murata, I., Nakajima, H., Palm, M., Paton-Walsh, C., Russell, J. M., Schneider, M., Servais, C., Smale, D., Walker, K. A.: Recent northern hemisphere stratospheric HCl increase due to atmospheric circulation changes, Nature, 515, 104-107, 10.1038/nature13857, 2014.

McPeters, R. D., Bhartia, P. K., Haffner, D., Labow, G. J., and Flynn, L.: The version 8.6 SBUV ozone data record: An overview, J. Geophys. Res. Atmos., 118, 8032-8039, doi:10.1002/jgrd.50597, 2013).

Molod, A., Takacs, L. L., Suarez, M. J., Bacmeister, J. T., Song, I.-S., and Eichmann, A.: The GEOS-5 Atmospheric General Circulation Model: Mean Climate and Development from MERRA to Fortuna. NASA Tech. Memo. 104606, Vol. 28, Tech. Rep. Series on Global Modeling and Data Assimilation, edited by: Suarez, M. J., 117 pp., 2012.

Molod, A., Takacs, L., Suarez, M. J., and Bacmeister, J. T.: Development of the GEOS-5 atmospheric general circulation model: evolution from MERRA to MERRA2, Geosci. Model Dev., 8, 1339–1356, 2015.

Oman, L. D., Douglass, A. R., Ziemke, J. R., Rodriguez, J. M., Waugh, D. W., and Nielsen, J. E.: The ozone response to ENSO in Aura satellite measurements and a chemistry-climate simulation, J. Geophys. Res., 118, 965-976, doi:10.1029/2012JD018546, 2013.

Park, J., Ko, M. K. W., Plumb, R. A., Jackman, C. H., Kaye, J. A., and Sage, K. H.: Report of the 1998 Models and Measurements II Workshop, NASA Tech. Publ., NASA/TM-1999-209554, 1999.

Pawson, S., and Steinbrecht, W. (Lead Authors), Charlton-Perez, A. J., Fujiwara, M., Karpechko, A. Yu, Petropavlovskikh, I., Urban, J. and Weber, M.: Update on global ozone: Past, present, and future, Chapter 2 in

Scientific Assessment of Ozone Depletion: 2014, Global Ozone Research and Monitoring Project – Report No. 55, World Meteorological Organization, Geneva, Switzerland, 2015.

Ploeger, F., Abalos, M., Birner, T., Konopka, P., Legras, B., Müller, R., and Riese, M.: Quantifying the effects of mixing and residual circulation on trends of stratospheric mean age of air, Geophys. Res. Lett., 2047–2054. doi: 10.1002/2014GL062927, 2015.

Polvani, L. M., Want, L., Aquila V., and Waugh, D. D.: The Impact of Ozone-Depleting Substances on Tropical Upwelling, as Revealed by the Absence of Lower Stratospheric Cooling since the Late 1990s, J. Climate, 30, 2523-2534, doi: 10.1175/JCLI-D-16-0532.1, 2017.

Ramanathan, V.: Greenhouse effect due to chlorofluorocarbons: climatic implications, Science 190, 50-52, doi:10.1126/science.190.4209.50., 1975.

Randel, W. J., and Wu, F.: A stratospheric ozone profile data set for 1979–2005: Variability, trends, and comparisons with column ozone data, J. Geophys. Res., 112, D06313, doi:10.1029/2006JD007339, 2007.

Randel, W. J., and Thompson, A. M.: Interannual variability and trends in tropical ozone derived from SAGE II satellite data and SHADOZ ozonesondes, J. Geophys. Res., 116, D07303, doi:10.1029/2010JD015195, 2011.

Ray, E. A., Moore, F. L., Rosenlof, K. H., Davis, S. M., Bönisch, H., Morgenstern, O., Smale, D., Rozanov, E., Hegglin, M., Pitari, G., Mancini, E., Braesicke, P., Butchart, N., Hardiman, S., Li, F., Shibata, K., and Plummer, D. A.: Evidence for changes in stratospheric transport and mixing over the past three decades based on multiple data sets and tropical leaky pipe analysis, J. Geophys. Res., 115, D21304, doi:10.1029/2010JD014206, 2010.

Ray, E. A., Moore, F. L., Rosenlof, K. H., Davis, S. M., Sweeney, C., Tans, P., Wang, T., Elkins, J. W., Bönisch, H., Engel, A., Sugawara, S., Nakazawa, T., and Aoki, S..: Improving stratospheric transport trend analysis based on SF_6 and CO_2 measurements, J. Geophys. Res. Atmos., 119, 14,110–14,128, doi:10.1002/ 2014JD021802, 2014.

Rayner, N. A., Parker, D. E., Horton, E. B., Folland, C. K., Alexander, L. V., Rowell, D. P., Kent, E. C., and Kaplan, A.: Global analyses of sea surface temperature, sea ice, and night marine air temperature since the late nineteenth century, J. Geophys. Res., 108(D14), 4407, doi:10.1029/2002JD002670, 2003.

Rienecker, M. M., Suarez, M. J., Roding, R., Bacmeister, J., Takacs, L., Liu, H.-C., Gu, W., Sienkiewicz, M., Koster, R. D., Gelaro, R., Stajner, I., and Nielsen, J. E.: The GEOS-5 data assimilation system—Documentation of versions 5.0.1, 5.1.0, and 5.2.0. Technical Report Series on Global Modeling and Data Assimilation, 27, 2008.

Rienecker, M. M, Suarez, M. J., Gelaro, R., Todling, R., Bacmeister, J., Liu, E., Bosilovich, M. G., Schubert, S. D., Takacs, L., Kim, G. K., Bloom, S., Chen, J. Y., Collins, D., Conaty, A., Da Silva, A., Gu, W., Joiner, J., Koster, R. D., Lucchesi, r., Molod, A., Owens, T., Pawson, Sl., Pegion, P., Redder, C. R., Reichle, R., Robertson, F. R., Ruddick, A. G., Sienkiewicz, M., Woollen, J.: MERRA: NASA's Modern Era Retrospective Analysis for Research and Applications, J. Clim., 24, 3624–3648, 2011.

Rinsland, C.P., Mahieu, E., Zander, R., Jones, N. B., Chipperfield, M. P., Goldman, A., Anderson, A., Russell III, J. M., Demoulin, P., Nothold, J., Toon, G. C., Blavier, J.-F., Sen, B., Sussman, R., Wood, S. W., Meier, A., Griffith, D. W. T., Chiou, L. S., Murcray, F. J., Stephen, T. M., Hase, F., Mikuteit, S., Schulz, A., and Blumenstock, T.: Long-term trends of inorganic chlorine from ground-based infrared solar spectra: Past increases and evidence for stabilization, J. Geophys. Res., 108, 4252, doi:10.1029/2002JD00300, 2003.

Roche, A. E., Kumer, J. B., Nightingale, R. W., Mergenthaler, J. L., Ely, G. A., Bailey, P. L., Massie, S. T., Gille, J. C., Edwards, D P., Gunson, M. R., Abams, M. C., toon, G. C., Webster, C. R., Traub, W. A., Jucks, K. W., Johnson, D. G., Murcray, D. G., Murcray, F. H., Goldman, A., and Zipf, E. C.: Validation of CH_4 and N_2O measurements by the cryogenic limb array etalon spectrometer instrument on the upper atmosphere research satellite, J. Geophys. Res., 101, 9679-9710, doi:10.1029/95JD03442, 1996.

Ronsmans, G., Langerock, B., Wespes, C., Hannigan, J. W., Hase, R., Kerzenmacher, T., Mahieu, E., Schneider, M., Smale, D., Hurtmans, D., De Maziere, M., Clerbaux, C., and Coheur, P. F.: First characterization and validation of FORLI-HNO_3 vertical profiles retrieved from IASI/Metop, Atmos. Meas. Tech., 9, 4783-4801, doi:10.5194/amt-9-4783-2016, 2016.

Russell III, J. M., Gordley, L. L., Park, J. H., Drayson, S. R., Hesketh, W. D., Cicerone, R. J., Tuck, A. F., Frederick, J. E., Harries, J. E., and Crutzen, P. J.: The Halogen Occultation Experiment, J. Geophys. Res., 98, 10777–10797, doi:10.1029/93JD00799, 1993.

Schauffler, S. M., Atlas, E. L., Donnelly, S. G., Andrews, A., Montzka, S. A., Elkins, J. W., Hurst, D. F., Romashkin, P. A., Dutton, G. S., and Stroud, V.: Chlorine budget and partitioning during the Stratospheric Aerosol and Gas Experiment (SAGE) III Ozone Loss and Validation Experiment (SOLVE), J. Geophys. Res., 108, 4173, doi:10.1029/2001JD002040, D5, 2003.

Schoeberl, M. R., Sparling, L. C., Jackman, C. H., and Fleming, E. L.: A Lagrangian view of stratospheric trace gas distributions, J. Geophys. Res., 105, 1537–1552, doi:10.1029/1999JD900787, 2000.

Schoeberl, M. R., Douglass, A. R., Polansky, B., Boone, C., Walker, K. A., and Bernath, P.: Estimation of stratospheric age spectrum from chemical tracers, J. Geophys. Res., 110, D21303, doi:10.1029/2005JD006125, 2005.

Shepherd, T. G., Plummer, D. A., Scinocca, J .F., Hegglin, M. I., Fioletov, V. E,. Reader, M. C., Remsberg, E., von Clarmann, T., and Wang, H. J.: Reconciliation of halogen-induced ozone loss with the total-column ozone record, Nature Geosci., 7, 443-449, doi: 10.1038/ngeo2155, 2014.

SPARC CCMVal, SPARC report on the Evaluation of Chemistry-Climate Models, Eyring, V., Shepherd, T. G., Waugh, D. W. (Eds.), SPARC Report No. 5, WCRP-132, WMO/TD-No. 1526, 2010.

Strahan, S.E., Duncan, B. N., and Hoor, P.: Observationally derived transport diagnostics for the lowermost stratosphere and their application to the GMI chemistry and transport model (2007), Atmos. Chem. Phys., 7, 2435-2445, 2007.

Strahan, S. E., Douglass, A. R., Stolarski, R. S., Akiyoshi, H., Bekki, S., Braesicke, P., Butchart, N., Chipperfield, M. P., Cugnet, D., Dhomse, S., Frith, S. M., gettelman, A., Hardiman, S. C., Kinnison, D. E., Lamarque, J.-F., Mancini, E., Marchand, M., Michou, M., Morgenstern, O., Nakamura, T., Olivié, D., Pawson, S., Pitari, G., Plummer, d. A., Pyle, J. A., Scinocca, J. F., Shepherd, T. G., Shibata, K., Smale, D., Teyssèdre, Tian, W., and Yamashita, Y.: Using transport diagnostics to understand chemistry climate model ozone simulations, J. Geophys. Res., 116, D17302, doi:10.1029/2010JD015360, 2011.

Strahan, S.E., Douglass, A.R., and Newman, P.A.: The contributions of chemistry and transport to low Arctic ozone in March 2011 derived from Aura MLS Observations, J. Geophys. Res., 118, doi:10.1002/jgrd.50181, 2013.

Strahan, S.E., Oman, L. D., Douglass, A. R., and Coy L.: Modulation of Antarctic vortex composition by the Quasi-Biennial Oscillation, Geophys. Res., Lett., 42, 10.1002/2015GL063759, 2015.

Strahan, S. E., Douglass, A.R., and Steenrod S.D.: Chemical and Dynamical Impacts of Stratospheric Sudden Warmings on Arctic Ozone Variability, J. Geophys. Res., 121, 11,836–11,851, doi:10.1002/2016JD025128, 2016.

Thompson, D. W. J., and Solomon, S.: Understanding Recent Stratospheric Climate Change, J. Climate, 22, 1934-1943, doi: 10.1175/2008JCLI2482.1., 2009.

Waugh, D. W., Strahan, S. E., and Newman, P. A.: Sensitivity of stratospheric inorganic chlorine to differences in transport, Atmos. Chem. Phys., 7, 4935-4941, doi:10.5194/acp-7-4935-2007, 2007.

Waugh, D. W., and Hall, T. M.: Age of stratospheric air: Theory, observations and models, Rev. Geophys., 40, 1-1 – 1-26, doi:10.1029/2000RG000101, 2002.

WMO (World Meteorological Organization), Scientific Assessment of Ozone Depletion: 2010, Global Ozone Research and Monitoring Project – Report No. 52, 516 pp., Geneva, Switzerland, 2011.

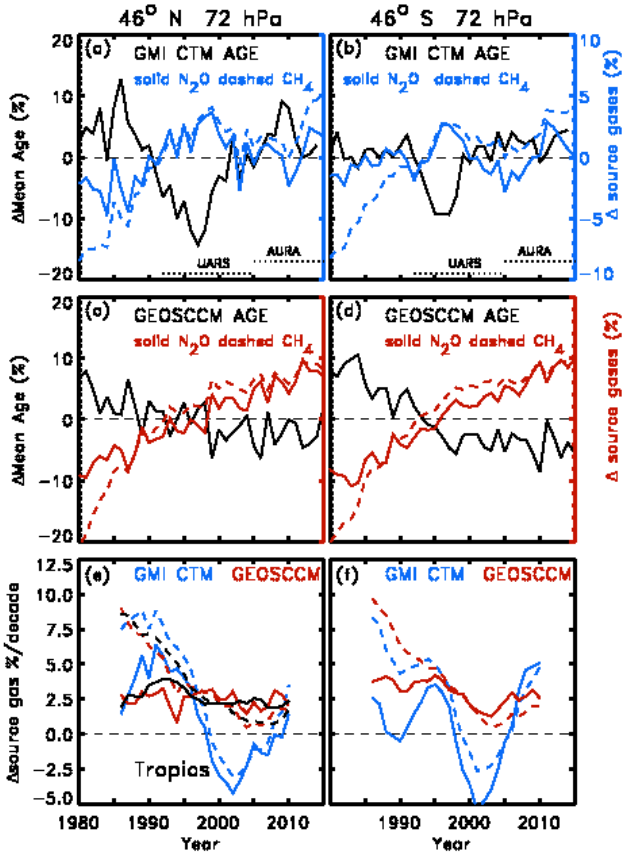

Figure 1: The GMI CTM differences from the 1980 – 2015 mean for mean age (black), N_2O (blue) and CH_4 (blue dashed) at 72 hPa for (a) 46° N and (b) 46° S. The GEOSCCM differences from the 1980 – 2015 mean for mean age (black), N_2O (red) and CH_4 (red dashed) at 72 hPa for (c) 46° N and (d) 46° S. Trends calculated for successive 10 year periods at 72 hPa are shown for N_2O (blue, GMI CTM; red GEOSCCM) and CH_4 (blue dashed, GMI CTM; red dashed GEOSCCM) at (e) 46° N and (f) 46° S. Tropical trends at 100 hPa (black, N_2O; black dashed CH_4) are shown in panel e). They are the same for both simulations and reflect the boundary conditions.

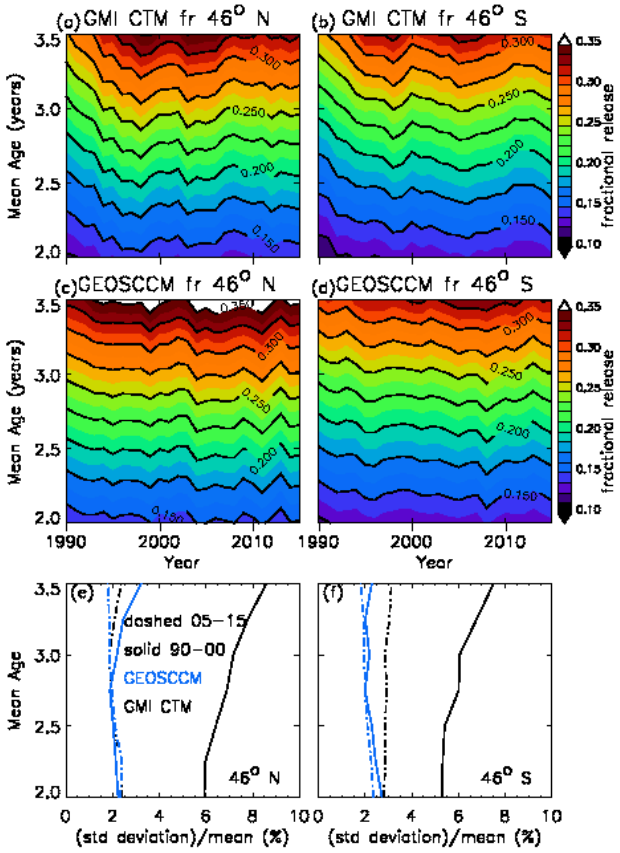

Figure 2: Contours of the evolution of N_2O fractional release simulated by GMI CTM for 1990 – 2015 as a function of mean age at (a) 46° N and (b) 46° S. Same for the GEOSCCM at (c) 46° N and (d) 46° S. The ratio of the standard deviation of the N_2O fractional release to the mean value from GMI CTM (black) and from GEOSCCM (blue) averaged from 1990 – 2000 (solid) and from 2005 – 2015 at (e) 46° N and (f) 46° S.

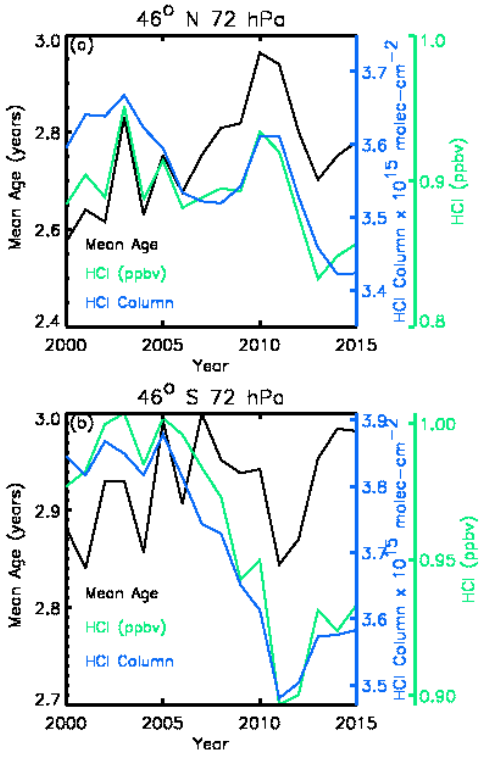

Figure 3: The evolution of the GMI CTM HCl mixing ratio (green) and mean age (black) at 72 hPa, and the HCl column (blue) at (a) 46° N and (b) 46° S. The HCl column is N x 10^{15} molecules per cm^2 where N is the blue right axis. The time interval begins in 2000 when the chlorine containing source gases have stopped increasing or begun to decline.

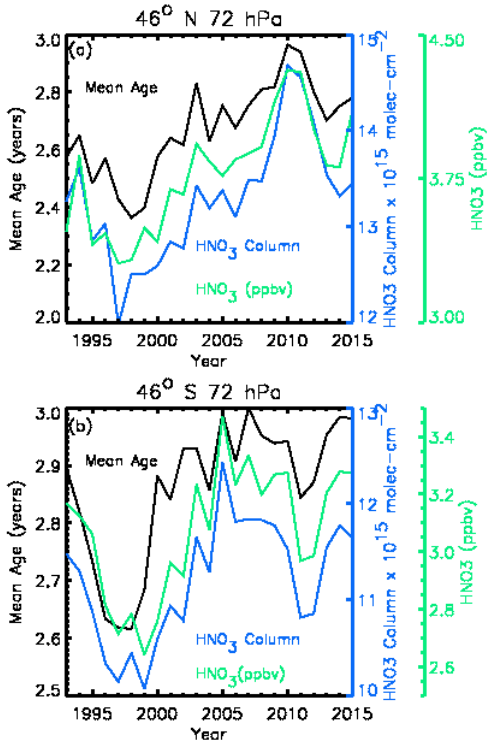

Figure 4: The evolution of the GMI CTM HNO_3 mixing ratio (green) and mean age (black) at 72 hPa, and the HNO_3 column (blue) at (a) 46° N and (b) 46° S. The HNO_3 column is N x 10^{15} molecules/cm^2 where N is the blue right axis. The time interval begins in 1993, about 18 months after eruption of Mt. Pinatubo.

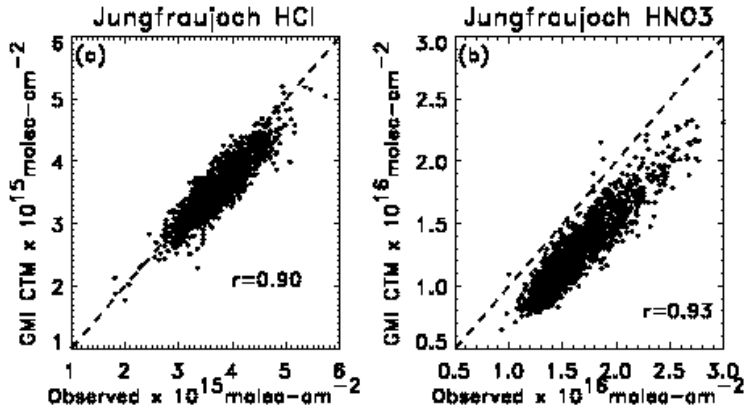

Figure 5: Simulated and observed columns 1989 – 2014 for (a) HCl and (b) HNO_3. Both simulated species are highly correlated with the observations when the simulation is sampled for the location and days of the measurements.

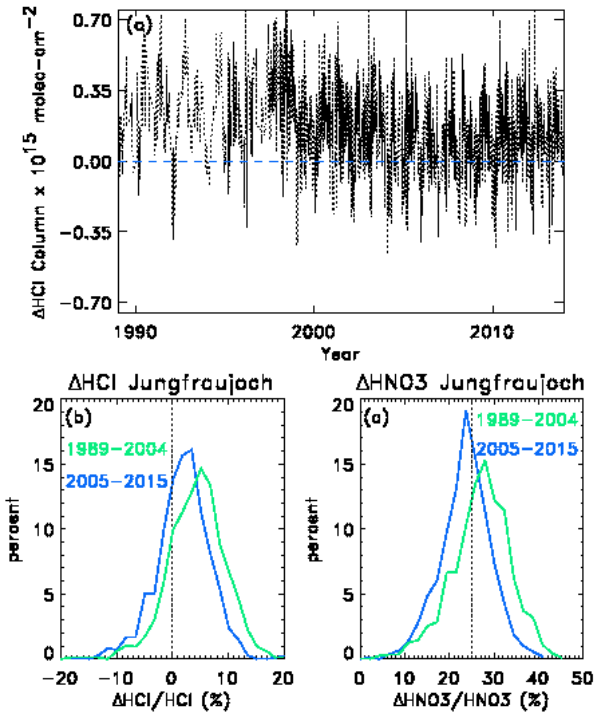

Figure 6: (a) Timeseries of the differences between observed and simulated HCl columns at Jungfraujoch. Histogram of the percentage differences for 1989-2004 (green) and 2005-2015 (blue) (b) for HCl and (c) HNO_3.

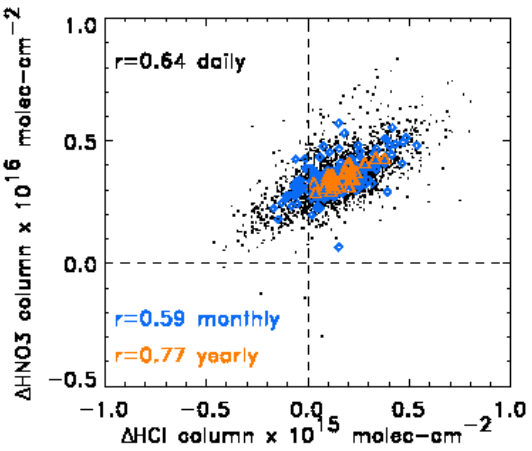

Figure 7: The differences between simulated and observed columns at Jungfraujoch for HCl are correlated with the differences for HNO_3 whether considering daily (black), monthly average (blue) or yearly average (orange) values.

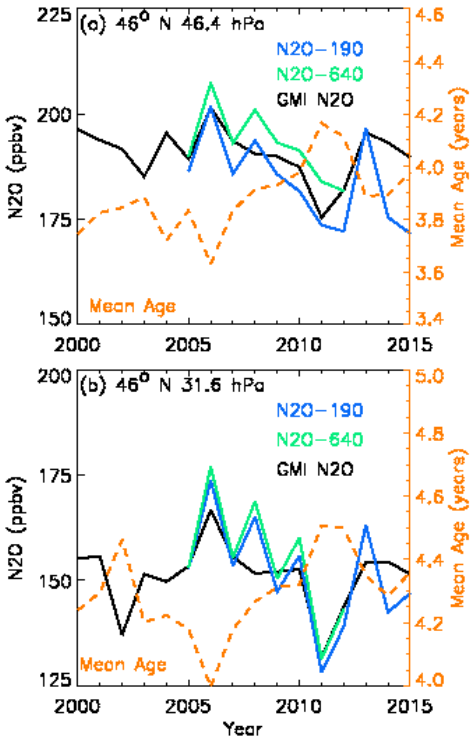

Figure 8: The 46° N annual zonal mean N_2O in the GMI CTM (black), the MLS N_2O-640 (green), the MLS N_2O-190 (blue), and the mean age (orange dashed) at (a) 46.4 hPa and; (b) 31.6 hPa. The simulated N_2O tracks the observed values and is anti-correlated with the mean age at both levels (-0.86 and -0.83 at 46.4 and 31.6 hPa respectively).

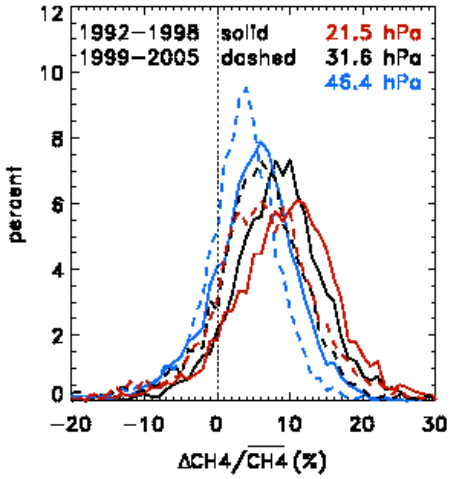

Figure 9: Histograms of percentage differences between HALOE and simulated CH_4 at 46.4 hPa (blue), 31.6 hPa (black) and 21.4 hPa (red) for all HALOE profiles between 35°-55° N. The distributions at all levels shift towards better agreement with observations for 1999-2005 compared with 1992-1998.

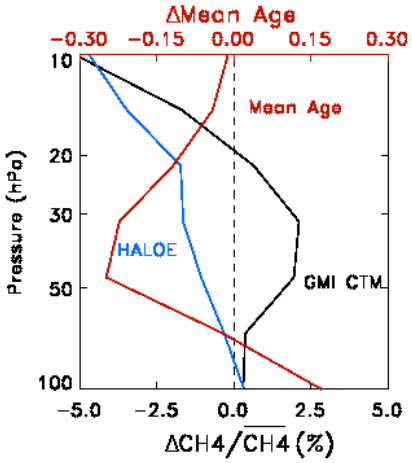

Figure 10: Percentage differences between 1994-1999 and 2000-2005 winter mean CH_4 profiles 35°-55° N for HALOE (blue) and GMI CTM (black). The difference between the 35°-55° N winter mean age profiles for the same periods is shown in red.

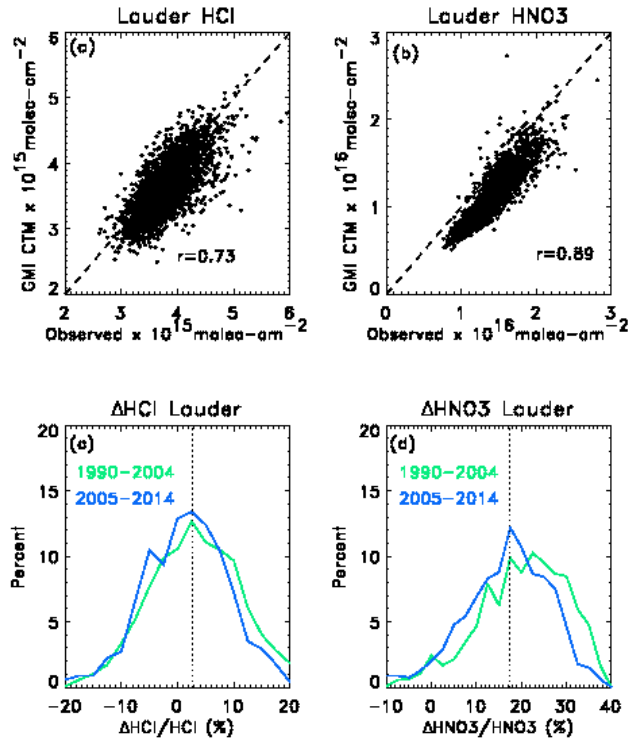

Figure 11: The GMI CTM and observed columns at Lauder station 1990 – 2014 for (a) HCl and (b) HNO_3. Histogram of the percentage difference between simulated and observed columns 1990–2004 (blue) and 2005-2014 (green) for (c) HCl and (d) HNO_3.

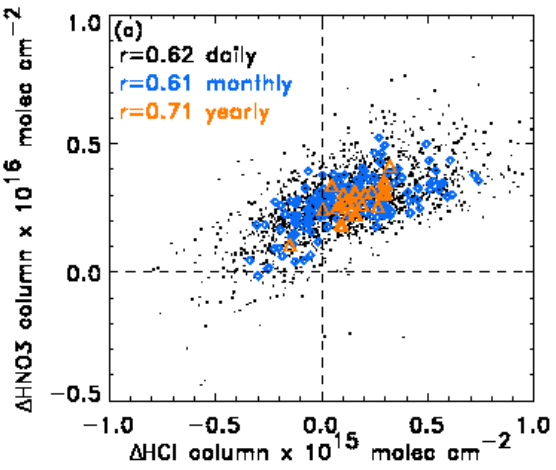

Figure 12: The differences between observed and simulated Lauder HCl columns are correlated with the differences between observed and simulated HNO_3 columns whether considering daily values (black), monthly averages (blue) or yearly averages (orange).

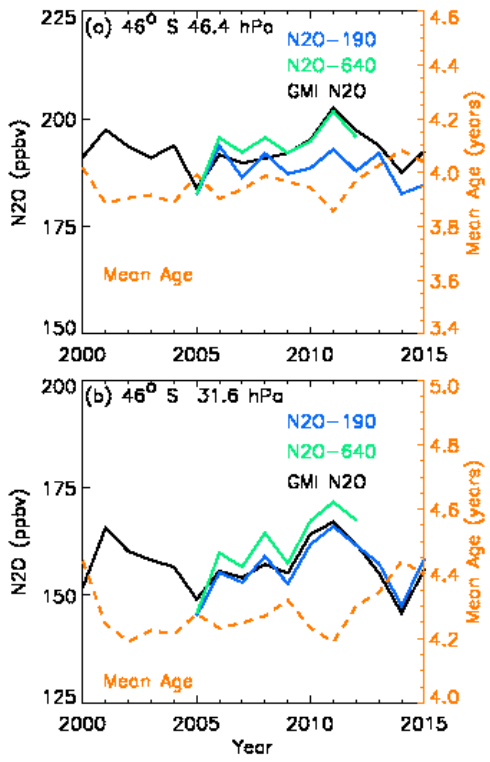

Figure 13: (a) The 46° S annual zonal mean N_2O in the GMI CTM (black) follows MLS N_2O-640 (green) but not N_2O-190 (blue) at 46.4 hPa. The simulated N_2O is anti-correlated with the mean age and with MLS N_2O-640. (b) The GMI CTM N_2O follows both MLS products 31.6 hPa, and is anti-correlated with mean age.

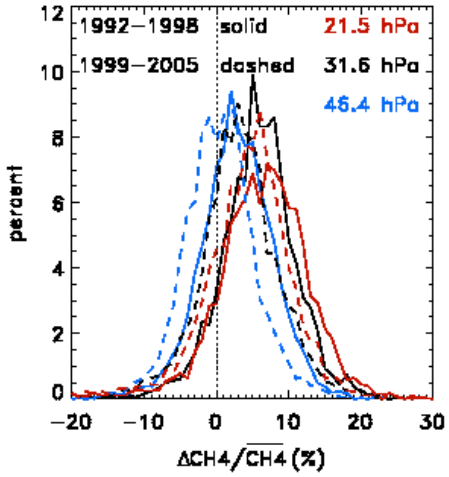

Figure 14: Histograms of percentage differences between HALOE and simulated CH_4 at 46.4 hPa (blue), 31.6 hPa (black), and 21.4 hPa (red) for all HALOE profiles between 35°-55° S for 1992-1998 (solid) and 1999-2005 (dashed).

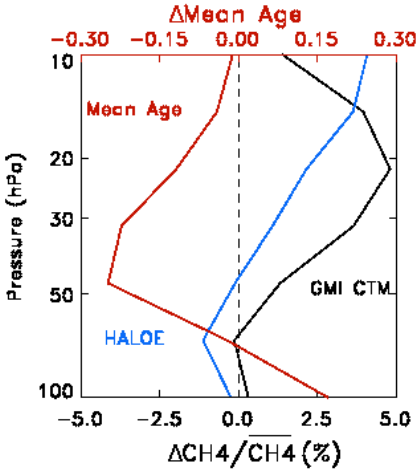

Figure 15: Percentage differences between 1994-1999 and 2000-2005 winter mean CH_4 profiles 35°-55° S for HALOE (blue) and GMI CTM (black). The difference between the 35°-55° S winter mean age profiles for the same periods is shown in red.